

# Equation of state effects and one-arm spiral instability in hypermassive neutron stars formed in eccentric neutron star mergers

William E. East<sup>1,2,\*</sup>, Vasileios Paschalidis<sup>3,†</sup>, Frans Pretorius<sup>3,‡</sup>

<sup>1</sup> Kavli Institute for Particle Astrophysics and Cosmology, Stanford University, SLAC National Accelerator Laboratory, Menlo Park, California 94025, USA

<sup>2</sup> Perimeter Institute for Theoretical Physics, Waterloo, Ontario N2L 2Y5, Canada

<sup>3</sup> Department of Physics, Princeton University, Princeton, NJ 08544, USA

\* E-mail: weast@perimeterinstitute.ca

† E-mail: vp16@princeton.edu

‡ E-mail: fpretori@princeton.edu

**Abstract.** We continue our investigations of the development and importance of the one-arm spiral instability in long-lived hypermassive neutron stars (HMNSs) formed in dynamical capture binary neutron star mergers. Employing hydrodynamic simulations in full general relativity, we find that the one-arm instability is generic in that it can develop in HMNSs within a few tens of milliseconds after merger for all equations of state in our survey. We find that mergers with stiffer equations of state tend to produce HMNSs with stronger  $m = 2$  azimuthal mode density deformations, and weaker  $m = 1$  components, relative to softer equations of state. We also find that for equations of state that can give rise to double-core HMNSs, large  $m = 1$  density modes can already be present due to asymmetries in the two cores. This results in the generation of  $l = 2$ ,  $m = 1$  gravitational wave modes even before the dominance of a one-arm mode that ultimately arises following merger of the two cores. Our results further suggest that stiffer equations of state give rise to HMNSs generating lower  $m = 1$  gravitational wave frequencies. Thus, if gravitational waves from the one-arm instability are detected, they could in principle constrain the neutron star equation of state. We estimate that, depending on the equation of state, the one-arm mode could potentially be detectable by second generation gravitational wave detectors at  $\sim 10$  Mpc and by third generation ones at  $\sim 100$  Mpc. Finally, we provide estimates of the properties of dynamical ejecta, as well as the accompanying kilonovae signatures.

PACS numbers: 04.25.D-, 04.30.Tv, 04.40.Dg, 07.05.Tp, 47.75.+f, 52.30.Cv, 95.75.Pq

## 1. Introduction

The LIGO and Virgo collaboration recently ushered in the era of gravitational wave (GW) astronomy with the observation of two high confidence signals that are both consistent with the inspiral and merger of binary black hole systems [2, 1]. This important milestone provides spectacular confirmation of the predictions of general relativity in the dynamical strong-field regime, the cleanest evidence yet for the existence of black holes, and gives important clues to the evolution of massive stars from inferred masses and limits on spins of the constituent black holes involved in the mergers. Over the next few years, it is anticipated that GWs will be observed not only from additional black hole binary mergers, but also from neutron star–neutron star (NSNS) and black hole–neutron star (BHNS) binary mergers.

Coalescing NSNSs and BHNSs are not only important sources of GWs, but may also be the progenitor systems that power short gamma-ray bursts [26, 49, 48, 9, 55]. In addition, these systems could generate other detectable electromagnetic (EM) signals, prior to [33, 44, 56, 51, 57, 47] and following [46, 45] merger. Combining GW and EM signals observed from such events could provide further precision tests of relativistic gravity, constrain the NS equation of state (EOS), and may help explain where the r-process elements in the Universe come from [61]. However, the interpretation of such “multimessenger” signals from compact binaries will be limited by our theoretical understanding of the processes involved. Gaining the requisite knowledge requires simulations in full general relativity (GR) because of the crucial role relativistic gravitation plays in such systems.

There have been multiple studies of compact binary mergers in full GR. For NSNSs, see [29, 3] for reviews and [54, 31, 20, 11, 50, 39, 16, 18, 15, 10, 64, 38, 52, 37, 10, 30, 32, 35, 62, 27, 59, 17, 65] for some more recent results. These earlier works have advanced our knowledge of EOS effects, neutrino transport, ejecta properties, jet outflows and magnetospheric phenomena. In addition, several studies (see e.g., [69, 6, 8, 7, 71, 72]) have investigated how GWs generated by oscillations of a hypermassive neutron star (HMNS) formed post-merger can be used to infer the nuclear EOS. These studies have focused primarily on the  $l = 2$ ,  $m = 2$  GW mode, which in terms of energy flux is the dominant component of the GW emission. However, the frequency of this mode is of order 2-3 kHz, outside the range where the advanced gravitational wave detectors have the most sensitivity.

In a recent work of ours [53], we discovered that a so-called one-arm spiral instability can develop in HMNSs formed in high-eccentricity dynamical capture binary neutron star mergers. Heuristically speaking, once saturated the one-arm instability manifests as a dense core offset from the center of mass about which it rotates at roughly constant frequency, and the  $m = 1$  azimuthal deformation of the rest-mass density distribution dominates over all other non-zero  $m$  modes. For more details on the history and features of the one arm spiral instability, and a discussion of dynamical capture versus field binaries, we refer the reader to [53, 19] and the references therein. This  $m = 1$

deformation of the rest-mass density generates  $l = 2$ ,  $m = 1$  GW modes. These  $(2, 1)$  GW modes from the instability are not initially as strong as the  $(2, 2)$  modes, but they have almost constant frequency and amplitude compared to the decaying  $(2, 2)$  modes. Moreover, the  $m = 1$  nature of these modes means that their GW frequency is half that of the corresponding  $m = 2$  modes, lying in a band where ground-based gravitational wave detectors are more sensitive. Hence if the HMNS and conditions driving the instability survive for long enough, the  $(2, 1)$  modes could eventually dominate the GW signal-to-noise.

In [19] we considered a range of NS spins and impact parameters, all corresponding to initially marginally unbound ( $e \approx 1$ ) equal mass ( $1.35M_\odot$  each) systems, and chose a single EOS. For this range of parameters we found that the one-arm instability develops when the total angular momentum at merger divided by the total mass squared is  $J/M^2 \sim 0.9 - 1.0$ . This range is relevant for quasi-circular NSNS binaries, and so we conjectured that the one arm instability should also manifest in quasicircular NSNS binaries if a HMNS forms post-merger. This was recently confirmed first by [58], and subsequently by [41] who studied quasi-circular mergers of equal-mass and unequal-mass irrotational NSNSs, respectively.

In this work, we continue our investigation of the relevance of the one-arm instability in HMNS remnants following eccentric NS mergers by expanding the parameter space of initial conditions and NS properties. In particular, we consider different equations of state, as well as unequal mass stars and different total masses for the binary. Our survey indicates that the one-arm spiral instability is generic in that it can be excited for all of the equations of state in our survey which form sufficiently long-lived HMNSs (i.e. which do not promptly collapse to black holes)<sup>‡</sup>. At this point it is important to clarify that while the term “instability” would normally imply a mode whose amplitude grows from some initial small seed, throughout we will use the term “one-arm spiral instability” to also imply the dominance of a “one-arm mode” (a nearly constant amplitude  $m = 1$  density mode) in the final HMNS, even when the initial  $m = 1$  “seed” is large, for e.g. when the binary mass ratio deviates significantly from unity.

We find that mergers with stiffer EOSs tend to produce HMNSs with stronger  $m = 2$  density deformations, and weaker  $m = 1$  components relative to softer EOSs. However, even for the stiffest EOS considered here, the HMNS can be dominated by a one-arm mode within a few tens of ms after merger. We also show that the EOS dependency of the size and oscillations of the resulting HMNS is imprinted in the frequency of the resulting GWs, which are sharply peaked in frequency space. In addition, we discover that the one-arm mode can dominate not only for equations of state that lead to toroidal and ellipsoidal HMNSs, but also for equations of state in which a double-core HMNS forms following merger. In this case, the one-arm mode dominates only after the two cores merge into one. Prior to merger of the two cores, the  $m = 2$  density mode

<sup>‡</sup> Though note that here we focus on impact parameters and initial NS spins that satisfy the criterion  $J/M^2 \sim 0.9 - 1.0$  prior to merger, identified in [19] as seeming to indicate when the remnant would be subject to the instability. Presumably here for the different EOSs and mass ratios similar criteria hold.

dominates in the cases considered here. However, small  $m = 1$  asymmetries at merger give rise to asymmetric cores in the double-core remnant which, like the one-arm mode, may act as quasi-stationary sources of  $l = 2$ ,  $m = 1$  GW modes.

As a side product we also estimate the properties of dynamically ejected matter, and find that for a given periapse distance unequal mass ratios eject more matter and the associated kilonovae signatures are brighter.

The remainder of the paper is organized as follows. In Section 2 we describe the equations of state we survey, the initial data, and the methods we adopt for evolving the Einstein and general relativistic hydrodynamic equations; in Sec. 3 we present the results from our simulations; and in Sec. 4 we conclude with a summary of our main findings and description of future work. Unless otherwise specified, below we adopt geometrized units where  $G = c = 1$ .

## 2. Methods

### 2.1. Initial conditions

As in [25, 53], we construct constraint-satisfying initial data for our evolutions starting from isolated rigidly-rotating equilibrium NS solutions that are generated with the code of [13, 14]. The free-data for the metric and matter fields are then determined by superposing two boosted isolated NS solutions, with the velocities and positions of a marginally unbound Newtonian orbit at a separation of  $d = 50M$  ( $\sim 200$  km; where  $M$  is the total ADM mass), and then solving the constraints. Here we consider the piecewise polytropic equations of state labelled “B”, “HB”, “H”, “2H” in [60], which yield maximum masses for nonspinning neutron stars — the Tolman-Oppenheimer-Volkov (TOV) limit — of  $2.06$ ,  $2.12$ ,  $2.25$ , and  $2.83 M_\odot$ , respectively. Of these equations of state, “B” is the softest, while “2H” is the stiffest one, where a stiffer equation of state yields a non-rotating neutron star of larger areal radius for the same gravitational mass. In addition, we consider a  $\Gamma = 3$  polytropic EOS. For the  $\Gamma = 3$  EOS specifically, we choose two different compaction stars, which when assigned the same gravitational mass ( $1.35M_\odot$ ) can be viewed as stars constructed with different equations of state corresponding to the same polytropic index, but different values for the polytropic constant. In particular, the values we choose are  $k_1 = 349981 \text{ km}^4$ , yielding a maximum TOV mass of  $2.06M_\odot$ , and  $k_2 = 460254 \text{ km}^4$ , yielding a maximum TOV mass of  $2.21M_\odot$ . Throughout we will refer to these as equations of state  $k_1$  and  $k_2$  respectively. To account for shock heating following merger, we also add a thermal component to the pressure:  $P_{\text{th}} = (\Gamma_{\text{th}} - 1)\epsilon_{\text{th}}\rho_0$  where  $\epsilon_{\text{th}}$  is the thermal part of the internal specific energy  $\epsilon$  and  $\rho_0$  is the rest mass density. We choose  $\Gamma_{\text{th}} = 1.5$  for all cases, except for the  $\Gamma = 3$  polytropic stars, which we evolve with a  $\Gamma$ -law EOS  $P = (\Gamma - 1)\epsilon\rho_0$  with  $\Gamma = 3.0$ §.

In Table 1 we list several properties of the NS models we consider in this work.

§ Though technically such an EOS can give superluminal sound speeds at sufficiently large values of  $\epsilon$ , we have checked that this does not occur for the cases considered here.

**Table 1.** Properties of isolated NS models considered in this work. Listed are the equation of state, dimensionless NS spin  $a_{\text{NS}}$ , spin period  $P_s$  in ms, rest mass  $M_0$  in  $M_\odot$ , ADM mass  $M_{\text{NS}}$  in  $M_\odot$ , circumferential equatorial radius  $R_{\text{NS}}$  in km, compaction  $C = M_{\text{NS}}/R_{\text{NS}}$ , and ratio of kinetic  $T$  to potential  $|W|$  energy.

EOS	$a_{\text{NS}}$	$P_s(\text{ms})$	$M_0(M_\odot)$	$M_{\text{NS}}(M_\odot)$	$R_{\text{NS}}(\text{km})$	$C$	$\frac{T}{ W } \times 100$
B	0.075	6.35	1.50	1.35	10.97	0.18	0.15
B	0.05	9.50	1.50	1.35	10.95	0.18	0.07
HB	0.05	10.85	1.41	1.28	11.60	0.16	0.06
HB	0.05	10.10	1.58	1.42	11.59	0.18	0.07
H	0.075	7.71	1.48	1.35	12.28	0.16	0.14
H	0.05	11.54	1.48	1.35	12.26	0.16	0.06
2H	0.075	11.28	1.45	1.35	15.23	0.13	0.13
2H	0.05	16.88	1.46	1.35	15.21	0.13	0.06
2H	0.05	17.46	1.37	1.28	15.17	0.12	0.05
2H	0.05	16.28	1.54	1.42	15.25	0.14	0.06
2H	0.075	9.72	1.87	1.70	15.37	0.16	0.14
2H	0.05	14.54	1.87	1.70	15.35	0.16	0.06
$k_1$	0.075	6.68	1.51	1.35	10.88	0.18	0.15
$k_1$	0.05	9.98	1.51	1.35	10.87	0.18	0.07
$k_2$	0.075	7.49	1.50	1.35	11.62	0.17	0.14
$k_2$	0.05	11.21	1.50	1.35	11.60	0.17	0.06

The spins of the stars we consider correspond to rotation periods of  $\sim 7 - 15$  ms which are the most likely rotation periods of observed pulsars in globular clusters [53]. The ratio of kinetic to gravitational potential energy is  $< 0.11$  for the rotating equilibria considered here, and thus all of these models are stable against the development both of the dynamical and the secular bar-mode instability [66, 68].

For the binary simulations considered here, we restrict ourselves to cases where the NS spin is aligned with the orbital angular momentum of the system.

## 2.2. Evolution techniques and diagnostics

We evolve the general relativistic hydrodynamic equations with the code of [24], which solves the Einstein field equations in the generalized-harmonic formulation with fourth-order accurate finite differences, and the hydrodynamic equations in conservative form using finite volume techniques as detailed in [23].

In the analysis below, and in particular for studying the evolution of the one arm instability in a HMNS that forms post-merger, we will use the complex azimuthal mode decomposition of the conserved rest-mass density integrated throughout the star

$$C_m = \int \rho_0 u^0 \sqrt{-g} e^{im\phi} d^3x, \quad (1)$$

where  $u^\mu$  is the fluid 4-velocity,  $g$  the determinant of the spacetime metric, and  $\rho_0$

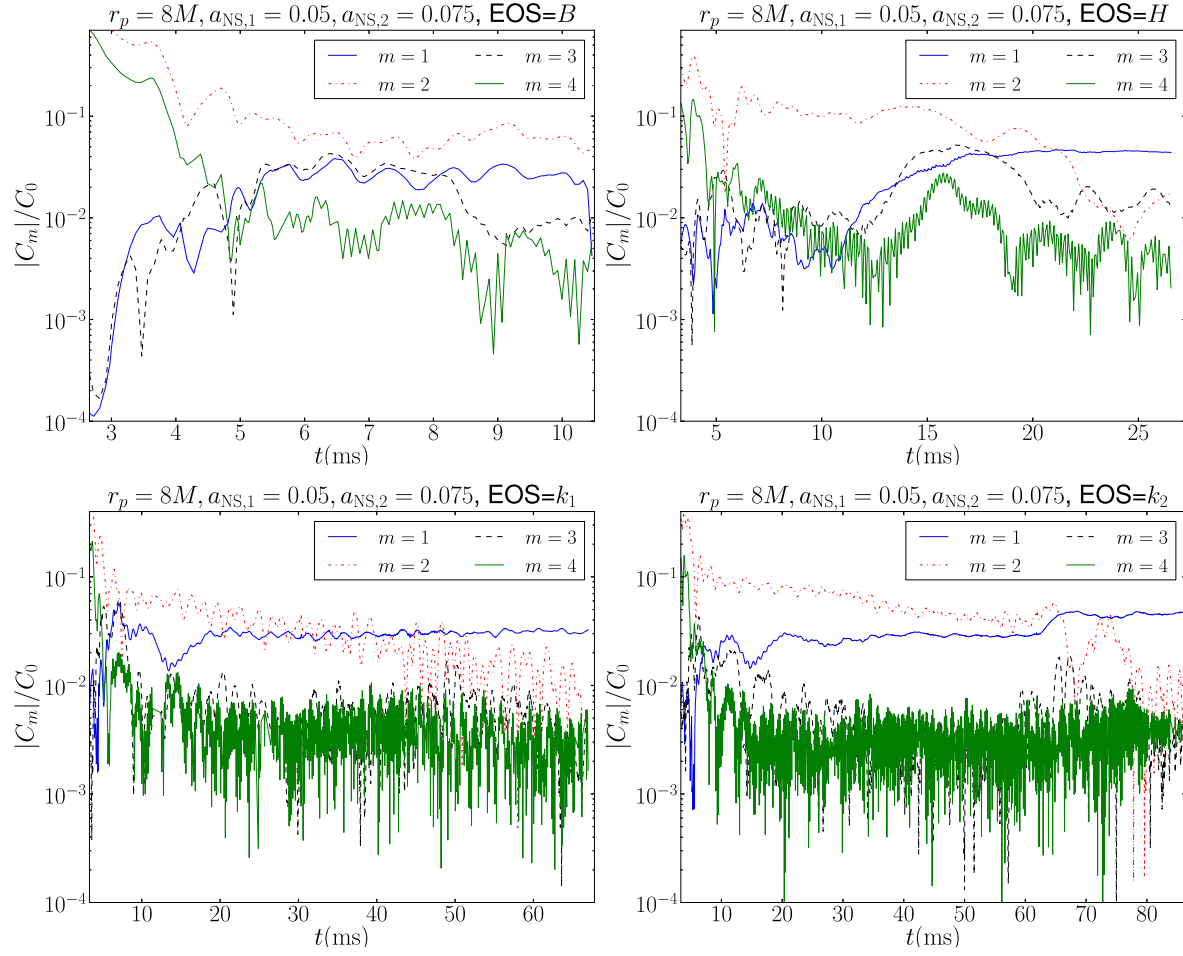


**Figure 1.** Amplitude of  $C_m$  normalized to  $C_0$  for various  $q = 1$  cases at  $r_p = 8M$ . (Note each panel covers a different time range).

the rest-mass density. We also track the coefficients  $C_{lm}(t, r)$  of the expansion of the Newman-Penrose scalar  $\Psi_4$  in spin-weighted spherical harmonics [5] defined as

$$C_{lm}(t, r) = \int d\Omega \, {}_{-2}Y_{lm}^*(\theta, \phi) \Psi_4(t, r, \theta, \phi), \quad (2)$$

where  $d\Omega$  stands for the differential solid angle,  ${}_sY_{lm}^*$  the complex conjugate of the spin-weighted spherical harmonics  ${}_sY_{lm}$ , with  $s = -2$  here.

### 3. Results

#### 3.1. Equation of state study in equal mass mergers

To begin with, we consider initial configurations in which each NS has a gravitational mass in isolation of  $1.35M_\odot$ , and initial orbital parameters corresponding to a (Newtonian orbit) periaapse distance  $r_p = 8M$ , and vary the EOS. We introduce a small asymmetry by letting one of the stars have a dimensionless spin of  $a_{\text{NS},1} = 0.05$ , and the other  $a_{\text{NS},2} = 0.075$ . For almost all the cases considered here, we find that



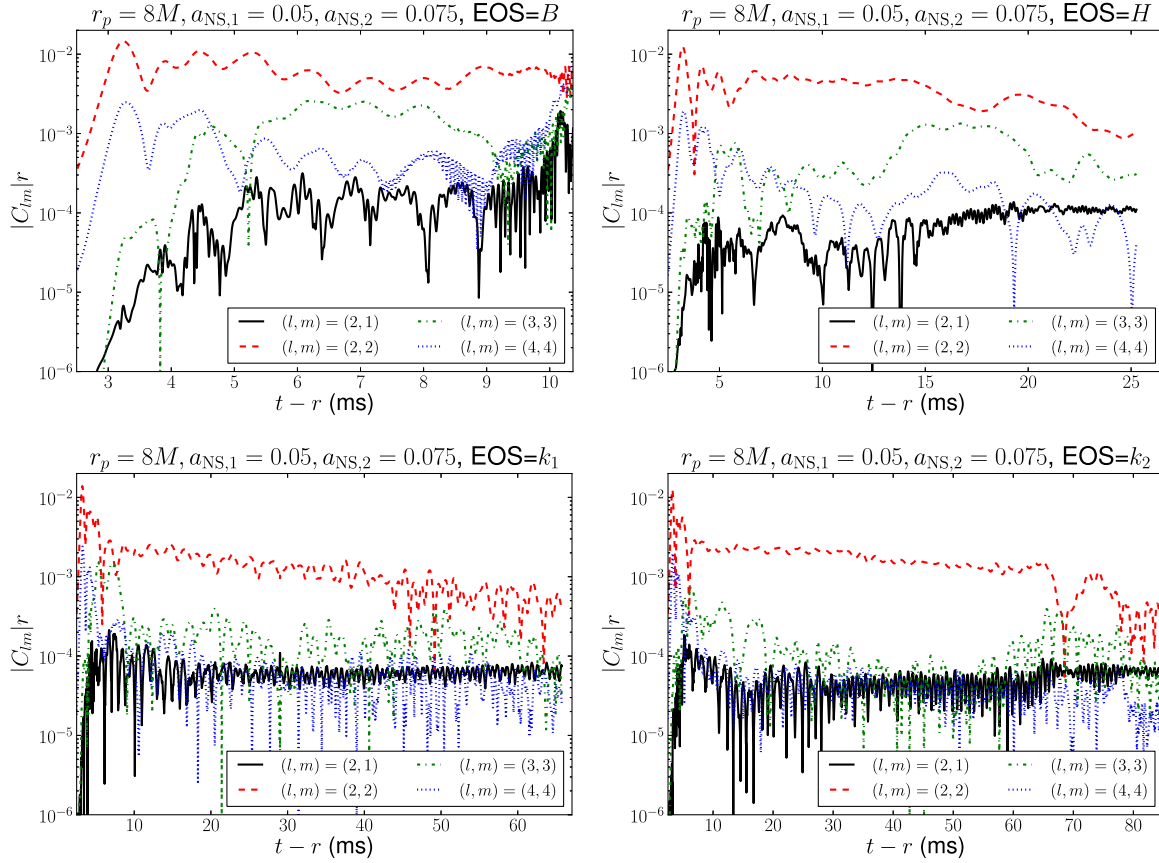


**Figure 2.** Amplitude of several spherical harmonic components of the GW signal, normalized by  $M$ , following merger. Each panel is from a case as shown in the corresponding panel of Fig. 1.

merger produces a long-lived hypermassive star that lasts the lifetime of the simulation, and furthermore that the  $m = 1$  instability is excited and eventually saturates in the same fashion as described in the introduction. The merger with the B EOS (the softest considered here) is the one exception that collapses to a BH during the time of the simulation, after  $\sim 10$  ms. In Fig. 1 we plot the amplitude of the azimuthal mode decomposition of the HMNS density versus time for some example cases, where it is clearly shown that, with the exception of the B EOS case, for sufficiently long evolutions the  $m = 1$  azimuthal modes dominate over all other non-zero modes. We plot the corresponding  $C_{lm}$ 's of the GWs in Fig. 2. Even when the  $m = 1$  mode dominates the density decomposition, it is still the  $l = 2, m = 2$  component of the oscillating HMNS that initially radiates the strongest GWs. This is at least in part responsible for the decay of the  $l = 2, m = 2$  mode with time. In contrast, in all cases where a clear one-arm mode dominates in the resulting HMNS, we see no evidence that the  $l = 2, m = 1$  GW mode decays; this is to be expected as long as conditions persist where the corresponding density mode of the NS is unstable. By the end of several of the simulations (including the unequal mass cases illustrated in Fig. 6) we find the  $C_{22}$  component is only a factor

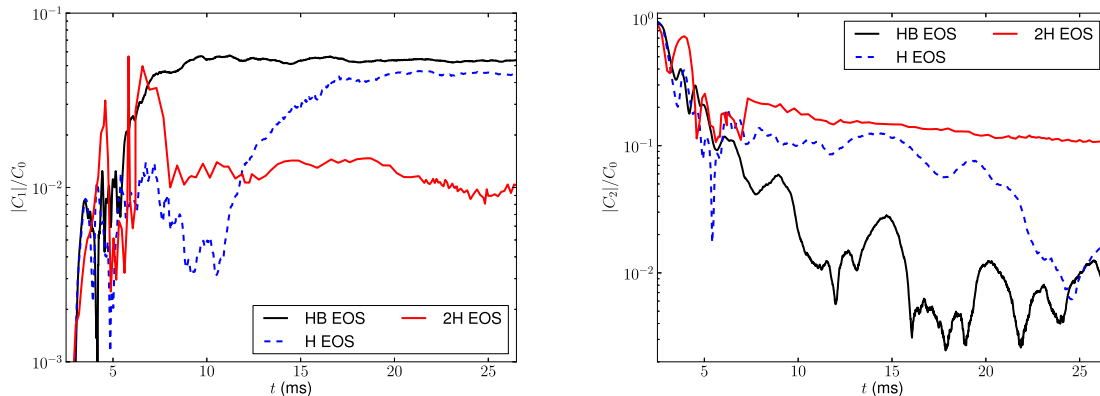


**Figure 3.** A comparison of the amplitude of the  $m = 1$  (left) and  $m = 2$  (right) density modes for equal-mass cases with  $r_p/M = 8$  and various EOSs.

of 1-4 times that of  $C_{21}$ . This implies that the  $l = 2, m = 1$  component of the GW strain  $h_{21}$  can become comparable to or larger than the  $l = 2, m = 2$  component  $h_{22}$ ; similarly for the energy  $E_{21}$  vs  $E_{22}$  carried by the corresponding GW modes. This is because for these near monochromatic GW sources  $h_{21}/h_{22} \propto (\Omega_{22}/\Omega_{21})^2 (C_{21}/C_{22}) \sim 4C_{21}/C_{22}$ , and  $E_{21}/E_{22} \propto (\Omega_{22}/\Omega_{21})^2 (C_{21}/C_{22})^2 \sim 4(C_{21}/C_{22})^2$ , with  $\Omega_{22}/\Omega_{21} \sim 2$  the ratio of the frequencies of the two modes.

In Fig. 3 we show a comparison of the  $m = 1$  and  $m = 2$  density modes for the different piece-wise polytropic EOSs that produce long-lived HMNSs (i.e. all of them except the B EOS), again focusing on equal-mass cases with the same impact parameter  $r_p = 8M$ . Here we can see that stiffer EOSs, which have more pressure support, develop and maintain larger  $m = 2$  modes and correspondingly smaller  $m = 1$  modes. While  $m = 1$  modes eventually dominate over the other nonzero density modes for the H and HB EOS, for the stiffest EOS considered here, the 2H, after  $\sim 35$  ms of evolution  $C_2/C_1 \sim 2$ . However, as we will discuss below, by considering larger impact parameters or unequal masses, we do find cases with the 2H EOS where the  $m = 1$  mode more strongly manifests.

In Table 2 we list the dominant frequencies of the  $m = 1$  and  $m = 2$  density modes that we obtain via a Fourier transform of  $C_1$  and  $C_2$ . As found before [53, 19], the frequencies satisfy  $f_{m=2} \approx 2f_{m=1}$ . Furthermore, stiffer EOSs mimicking realistic ones seem to produce lower frequency  $m = 1$  and  $m = 2$  modes. Although this is not as clean in the azimuthal mode decomposition of the density (possibly because of sparse sampling of the modes), it is more cleanly reflected in the GW spectrum (see below).

### 3.2. Double-core HMNSs

For the cases with the  $k_1$  and  $k_2$  EOSs, we find that a double-core HMNS forms post-merger, i.e. there are two distinct maxima in the density of the star. This is illustrated in Fig. 4 where we show snapshots of density contours and the velocity flow from



**Table 2.** From left to right the columns correspond to the equation of state, the pericenter distance, the dimensionless spins of the two stars, the masses of the two stars in units of  $M_\odot$ , and the dominant frequencies of the  $m = 1$  ( $f_{m=1}$ ) and  $m = 2$  ( $f_{m=2}$ ) modes in units of kHz. The last column indicates the approximate time after merger, in ms, at which the one-arm mode dominates the  $m > 1$  density modes (or a lower bound if this do not occur by the end of the simulated time). Apart from the B equation of state, which collapses to a BH, all other cases form “long-lived” hypermassive neutron stars to which the results correspond. We also include a lower resolution (2H,LR) run of one of our cases with the 2H EOS.

EOS	$r_p$	$a_{\text{NS},1}$	$a_{\text{NS},2}$	$M_{\text{NS},1}$	$M_{\text{NS},2}$	$f_{m=1}$	$f_{m=2}$	$T_{\text{one-arm}}$
$k_1$	8M	0.05	0.075	1.35	1.35	1.6	3.1	45
$k_2$	8M	0.05	0.075	1.35	1.35	1.5	2.9	62
H	8M	0.05	0.075	1.35	1.35	1.7	3.1	18
HB	8M	0.05	0.075	1.35	1.35	1.7	3.3	6
2H	8M	0.05	0.075	1.35	1.35	1.1	2.0	> 28
HB	8M	0.05	0.05	1.28	1.42	1.8	3.6	8
2H	8M	0.05	0.05	1.28	1.42	1.0	1.9	38
2H,LR	8M	0.05	0.05	1.28	1.42	1.0	2.0	12
2H	9.5M	0.05	0.05	1.35	1.35	1.1	1.9	17
2H	8M	0.05	0.05	1.70	1.70	1.1	2.3	> 33

the evolution of the  $r_p = 8M$ ,  $a_{\text{NS},1} = 0.05$ ,  $a_{\text{NS},2} = 0.075$ ,  $k_1$  case. In particular, following merger the two dense cores rotate around the common center of mass, which is surrounded by an underdense region (upper row in Fig. 4). One of the two cores is slightly larger than the other due to the initial  $m = 1$  asymmetry. The subsequent evolution is such that matter from the smaller core gradually flows towards that of the larger core until eventually the two cores merge into one. At this time the  $m = 1$  instability is clearly visible in the  $C_m$  modes in that  $|C_1| > |C_m|$ ,  $m = 2, 3$ , and 4.

In previous works, we reported that the background about which the one-arm instability develops was a toroidal-like HMNS (maximum density occurring in a ring around the center of mass on the equatorial plane), that formed following the interaction of post-merger fluid vortices arising at the shear layers near the surface of stars and the tidal tails during merger. Here, for many of the piece-wise polytropic EOS cases we do not find the same vortex dynamics as in our previous work, and the HMNS instead forms an ellipsoidal configuration, but is still subject to the  $m = 1$  instability. This is also the case for quasi-circular binary NS mergers reported in [58]. For the  $k_1$  and  $k_2$  polytropic EOS we find a third background: a double-core HMNS. This suggests that such details of the structure of the remnant do not play a significant role in determining whether conditions are ripe for eventual growth of the  $m = 1$  mode.

In the double core case, an asymmetry in the mass of the two cores causes a large  $m = 1$  mode to be present well before the cores merge and the one arm mode manifests. This is then another way strong  $l = 2$ ,  $m = 1$  gravitational-wave modes can be generated.

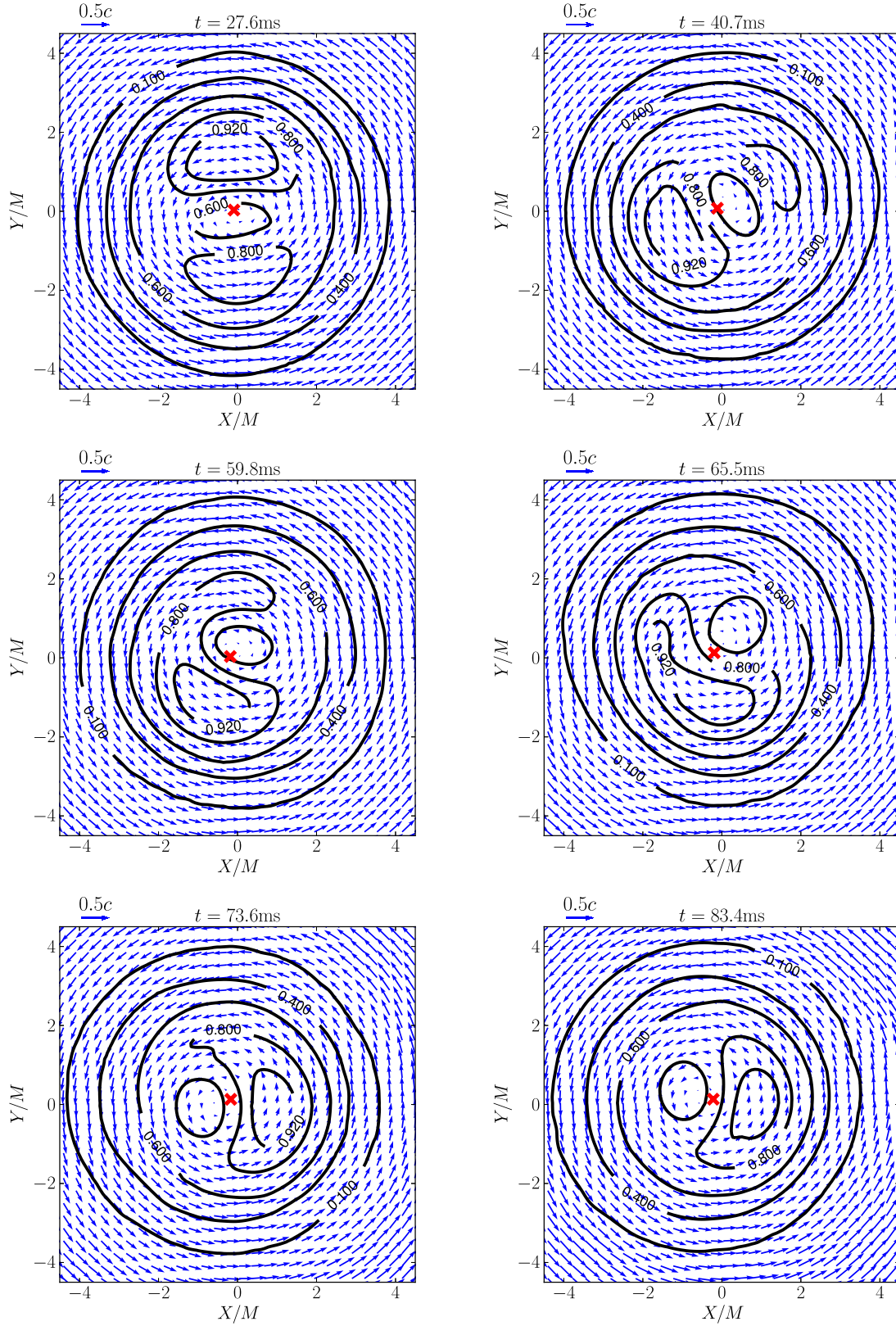


**Figure 4.** Contours of rest-mass density normalized to its maximum value (black solid lines) and coordinate velocity (arrows) on the equatorial plane at select times following merger. The (red) “x” indicates the HMNS center of mass. The data in all plots are taken from the  $r_p/M = 8$ ,  $a_{\text{NS},1} = 0.05$ ,  $a_{\text{NS},2} = 0.075$ ,  $k_2$  case.

Thus, detection of a near quasistationary  $l = 2$ ,  $m = 1$  GW signal may not necessarily imply the one-arm spiral instability. However, the results here suggest this degeneracy could be broken if one folds in information from the  $l = 2$ ,  $m = 2$  GW modes, which appear to be much stronger than the  $l = 2$ ,  $m = 1$  GW modes during the double core phase.

The  $\Gamma = 3$  polytropic stars we consider as our initial data here are evolved with a  $\Gamma$ -law EOS. This implies that  $\Gamma_{\text{th}} = 3$ . While this choice of  $\Gamma_{\text{th}}$  is large compared to what is typically adopted in the literature, it likely does not affect the physics of high-density matter that gives rise to the double cores, whose densities are approximately the same as the initial maximum density in the stars. The reason is that strong shock heating here (and hence high thermal pressure) occurs only in low density matter. For example using Eq. B6 of Appendix B in [28] and setting  $\Gamma = 3$  with  $k\rho^2 \sim 0.4^2$  (which holds for our  $\Gamma = 3$  models), one finds that in the strong shock limit the ratio of total pressure to cold pressure for our models is  $K \sim 0.06(v/0.4)^2(\rho_{0,\text{max}}/\rho_0)^2$ , where  $v$  is the collision velocity. Thus, only for rest-mass densities  $\rho_0 < 0.1\rho_{0,\text{max}}$  can there be a significant shock heating effect. But, since a  $\Gamma = 3$  EOS is stiff the bulk of the total neutron-star mass lies in the density range  $\rho_0 > 0.1\rho_{0,\text{max}}$ .

While our limited set of simulations cannot rule out the possibility that the double-core remnant arises due to the high value of  $\Gamma_{\text{th}}$ , we point out that double-core HMNS remnants are known to form even for lower values  $\Gamma_{\text{th}} = 1.357$  [34]. Thus, the results from our simulations employing a  $\Gamma$ -law with  $\Gamma = 3$  should simply be viewed as a qualitative representation of a class of EOSs for which binary neutron star mergers lead to the formation of double core HMNSs.

### 3.3. Effects of varying mass ratio and other parameters

In addition to the equal mass cases considered above, we also consider two cases with mass ratio  $q = 0.9$ . We use two equations of state, the HB and 2H, covering a range of stiffness from moderate to very stiff EOS, while keeping the total gravitational mass fixed to  $2.7M_\odot$ , the periaapse distance fixed to  $r_p = 8M$ , and the individual NS dimensionless spins fixed to 0.05. By virtue of the unequal mass-ratio, there is a strong  $m = 1$  component to the initial data. We find that the  $m = 1$  instability occurs in both cases. In Fig. 5 we plot the amplitude of  $|C_m|$  as a function of time demonstrating the dominance of the  $m = 1$  azimuthal modes. The plots demonstrate that soon after merger the  $m = 1$  mode reaches saturation, while the  $m = 2$  mode decays and eventually its amplitude drops below that of the  $m = 1$  mode, at which point the  $m = 1$  structure is clearly seen in 2D equatorial density plots. The corresponding decomposition of the GWs is shown in Fig. 6.

*3.3.1. Varying other parameters with the 2H EOS:* Above we showed that while the equal-mass 2H EOS case exhibited a strong  $m = 2$  mode and suppressed  $m = 1$  mode in the post-merger HMNS, the  $m = 1$  mode was noticeably enhanced in the  $q = 0.9$  case.

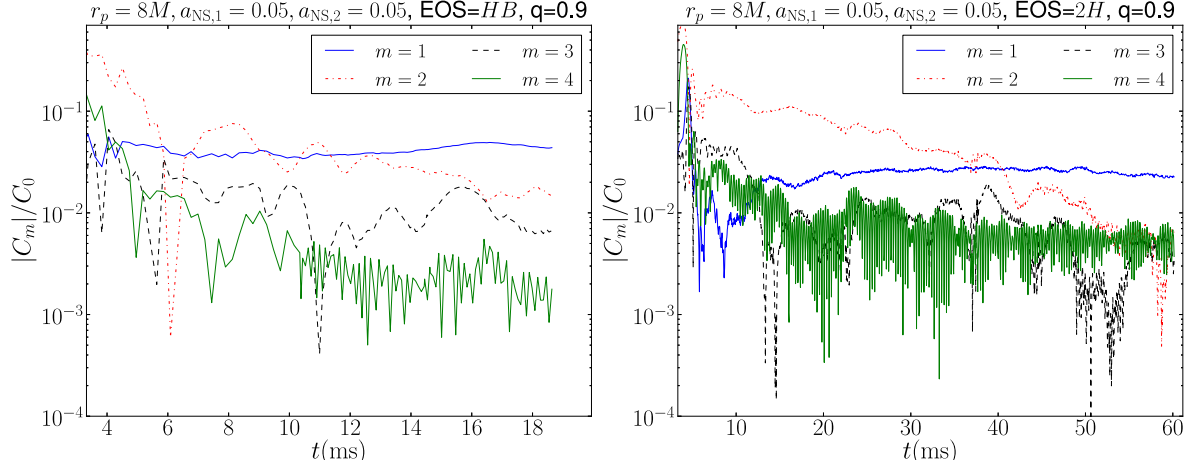


**Figure 5.** Amplitude of  $C_m$  normalized to  $C_0$  for  $q = 0.9$  cases (note the different time ranges for each plot).

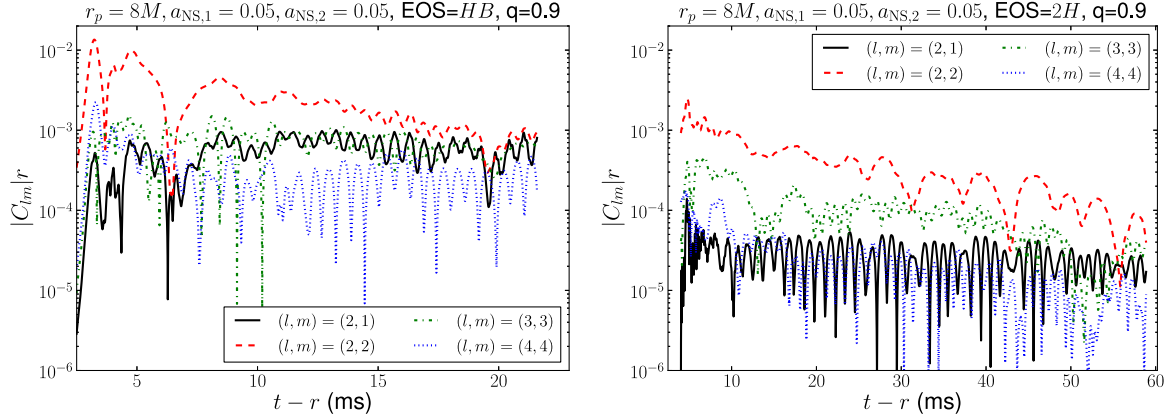


**Figure 6.** Amplitude of several spherical harmonic components of the GW signal, normalized by  $M$ , following merger for the same cases shown in corresponding panels in Fig. 5.

To probe the effects of the other binary parameters, we also consider equal-mass cases with this EOS where we increase the impact parameter to  $r_p = 9.5M$ , and hence the angular momentum at merger; we further examined a case where we increase the total mass of each NS from  $1.35$  to  $1.7 M_\odot$ , giving more compact stars. The  $m = 1$  and  $m = 2$  density modes from all four cases with the 2H EOS are compared in Fig. 7. The increased impact parameter does noticeably enhance the strength of the one-arm mode. On the other hand, the case with higher mass stars shows a significantly smaller  $m = 1$  mode. We find that when evolved to  $\approx 36$  ms, the  $m = 2$  mode decays noticeably, though it still dominates over the  $m = 1$  mode by roughly a factor of two.

Finally, based on the results listed in Table 2, we conclude that for a given total mass there is little variation ( $\sim 10\%$ ) of the mode frequencies when varying the mass ratio, the NS spins and the pericenter distance in the 2H EOS. The approximate independence

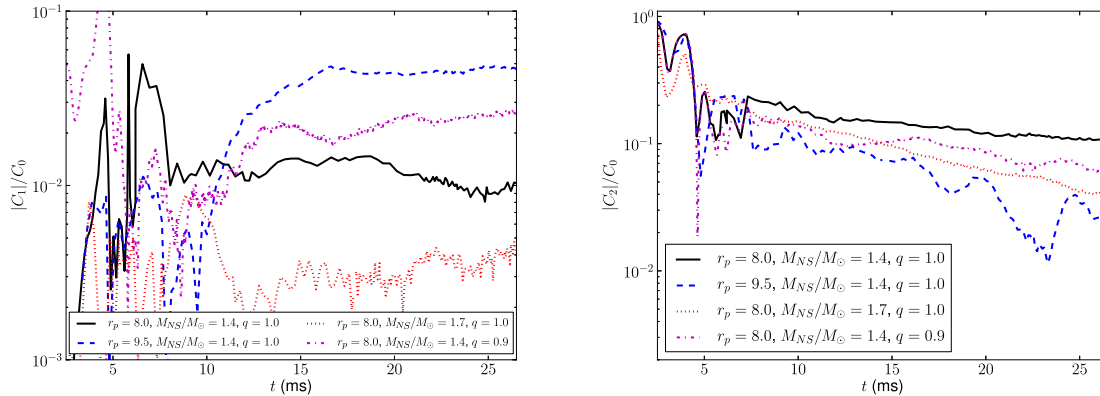


**Figure 7.** A comparison of the amplitude of the  $m = 1$  (left) and  $m = 2$  (right) density modes for various cases with the 2H EOS.

of the mode frequency with the mass ratio has also been reported in [41]. Given that the density-mode frequencies are reflected in the gravitational wave spectrum (see below), the small variation of the GW frequencies with these different binary parameters spells good news for the ability to constrain the nuclear EOS with future GW observations, as the HMNS oscillations seem to be largely determined by the total mass and the equation of state (at least within the context of our high-eccentricity mergers). However, detailed investigations are required to draw robust conclusions and derive high-accuracy results that can be useful for future GW observations. Such investigations will be the subject of future work of ours.

*3.3.2. Effects of resolution:* Resolution studies demonstrating the convergence properties of the solution for HB EOS cases were presented in [19]. Here we supplement this with an additional 2H EOS,  $q = 0.9$  case run at a resolution 0.64 times lower than the resolution for the other results above. The density mode analysis and the GWs from this case are shown in Fig. 8. The most notable feature in the lower resolution run is that the  $m = 2$  density modes decay much faster than in the higher resolution run, as does the  $l = 2$ ,  $m = 2$  mode of the GWs. As a result the  $m = 1$  instability manifests earlier in the lower resolution run. These results indicate that for accurate computation of all quantitative hydrodynamic effects higher resolution would need to be adopted; however, the appearance and qualitative nature of the  $m = 1$  instability, such as the approximately constant amplitude of the  $l = 2$ ,  $m = 1$  GW mode, appears relatively insensitive to resolution. Moreover, the frequencies of the density modes (see Table 2) agree to within 5% between the two different resolutions we adopt in the 2H  $q = 0.9$  case.



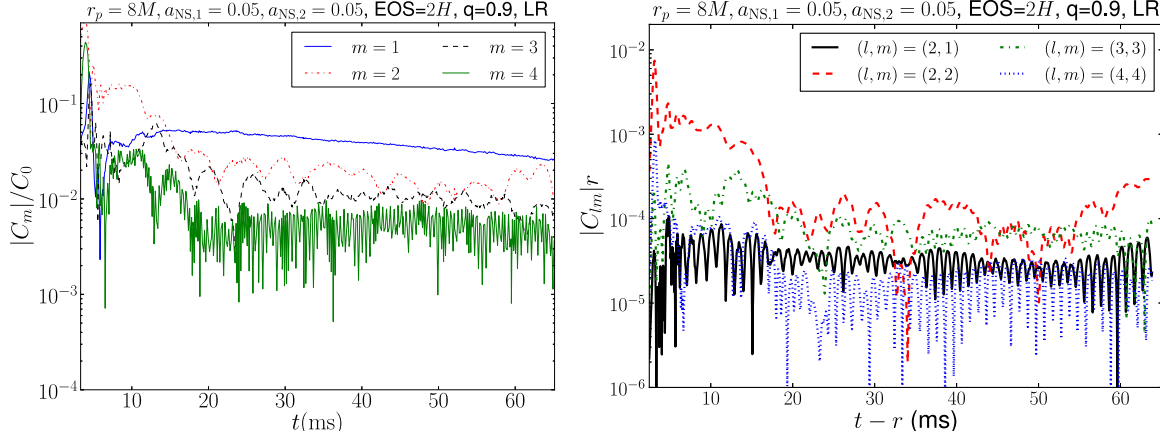


**Figure 8.** Results from a lower resolution run of the  $q = 0.9$ , 2H EOS case. Left: Amplitude of  $C_m$  normalized to  $C_0$  (compare right panel of Fig. 5). Right: Amplitude of several spherical harmonic components of the GW signal following merger (compare right panel of Fig. 6) .

### 3.4. Gravitational wave spectrum

The properties of the oscillating HMNS are encoded in the gravitational wave spectrum post-merger. In Fig. 9 we plot the characteristic GW strain  $h_c = |\tilde{h}|f$ , defined in terms of the Fourier transform  $\tilde{h}$  of the strain and frequency  $f$ . We show an integration of 10 ms post-merger for a consistent comparison amongst the various cases. In Fig. 9 we show the strain both as it would be measured by an observer on axis, where the  $(l, m) = (2, 2)$  will be maximal and the  $(2, \pm 1)$  modes will vanish, and by an observer on edge. In particular, in the on-edge plots a series of peaks can be seen at integer multiples of the frequency of the oscillation of the NS. The strongest peak corresponds to the dominant  $(l, m) = (2, 2)$  mode (at roughly 2 kHz for the 2H EOS, and  $\sim 3$  kHz for the softer EOSs), with the subdominant  $(2, 1)$  mode at roughly half the  $(2, 2)$  mode's frequency, hence in a more sensitive regime for GW detectors. As expected, the cases with softer EOSs, and thus more compact stars, have higher frequency peaks. Likewise the one case where the two NSs have a larger mass of  $1.7 M_{\text{odot}}$  has a higher frequency compared to the equivalent case where the NSs have a mass of  $1.35 M_{\text{odot}}$ . Again, the fact that the stiffer EOSs have weaker GWs coming from the  $m = 1$  oscillations is somewhat offset by the fact that the sensitivity is higher at lower frequencies. For fixed total mass, changing the mass-ratio or the impact parameter has a relatively small effect on the frequency of the GWs emitted in this time window after merger.

The hypermassive NSs can continue to emit GWs for much longer times than the 10 ms windows used for Fig. 9, building more power in the frequency ranges associated with the one-arm mode frequency and its integer multiples. This is illustrated in Fig. 10 where we compare the characteristic gravitational wave strain for two cases, but for much longer integration times. From this it can be seen that after the violence of the phase immediately following the merger, the GW power is concentrated into very narrow



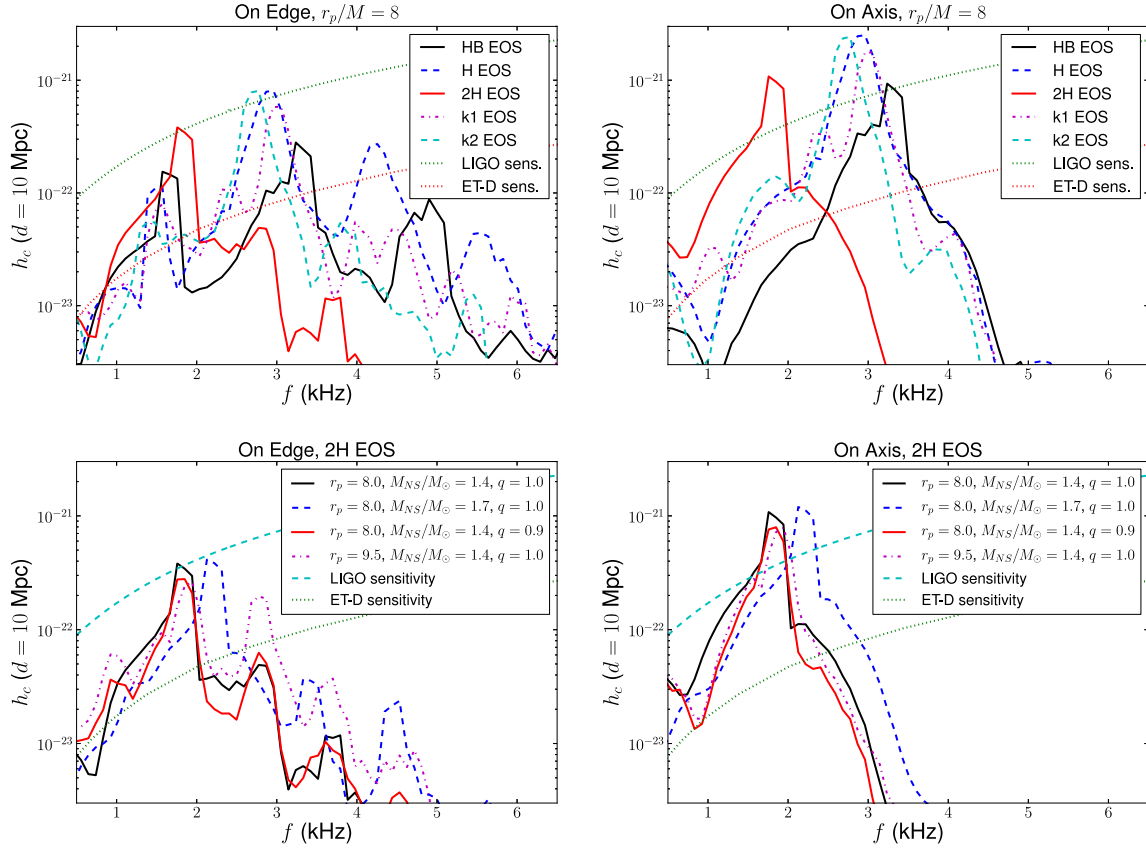


**Figure 9.** The characteristic gravitational wave strain as a function of frequency for an observer on edge (left panels) and on axis (right panels) for  $\approx 10$  ms of the post-merger phase. The top panels show equal-mass cases with  $r_p/M = 8$  and various EOSs while the bottom panels show various cases with the 2H EOS. We also show the sensitivity curves for the aLIGO and Einstein Telescope (ET) detectors.

frequency ranges, indicative of near monochromatic emission at distinct frequencies, and the integrated power can grow significantly for a long-lived HMNS. In Fig. 10 we have also included the sensitivity curve for a proposed “High Frequency” configuration for aLIGO that increases sensitivity in a narrow range at around 1 kHz [67], that happens to coincide with the  $m = 1$  mode frequency for the 2H EOS. Hence, if future observations indicate a favorable binary NS merger rate, such high frequency configurations may be worth considering to learn more about the post-merger dynamics, and potentially reveal information regarding the NS EOS.

We can estimate the approximate strength of the long-lived GW signals as follows. Assuming that: a) the source is observed on edge and b) the  $m = 1$  mode has constant frequency and amplitude, the signal-to-noise ratio (SNR) for the  $m = 1$  mode can be estimated via Eq. (81) of [36] (see also [41]) and approximating the 2,1 mode GW strain as  $h_{21} \sim C_{21}/(2\pi f_{m=1})^2$

$$\text{SNR}_{\text{aLIGO}} \approx 2.8 \left( \frac{7 \times 10^{-24} \text{Hz}^{-1/2}}{\sqrt{S_n(f_{m=1})}} \right) \left( \frac{C_{21} r M}{10^{-4}} \right) \left( \frac{1.5 \text{kHz}}{f_{m=1}} \right)^2 \left( \frac{T_{m=1}}{100 \text{ms}} \right)^{1/2} \left( \frac{10 \text{Mpc}}{r} \right) \quad (3)$$

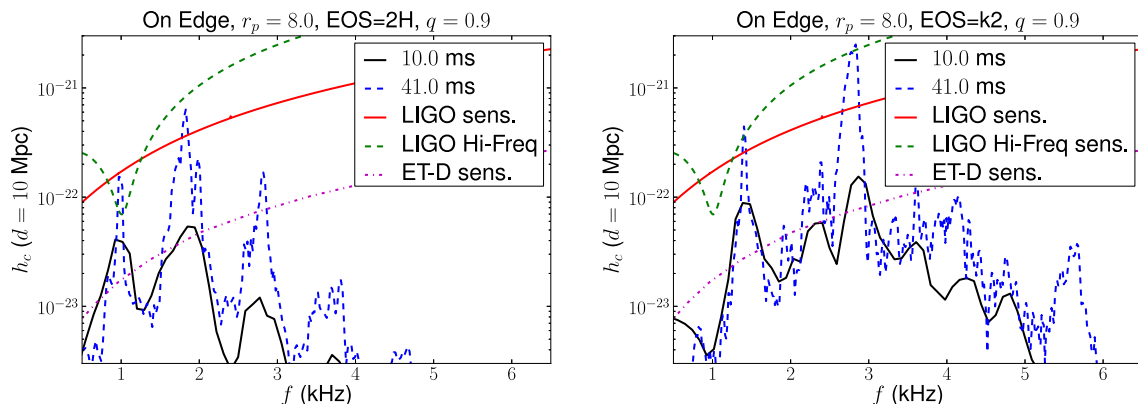


**Figure 10.** The characteristic gravitational wave strain as a function of frequency for an observer on edge comparing  $\approx 10$  ms of the post-merger phase to the full time simulated ( $\approx 41$  and  $65$  ms, for the right and left panels, respectively) for a case with the 2H EOS and  $q = 0.9$  (left) and the  $k_2$  EOS and  $q = 1$  (right). In addition to the sensitivity curves for aLIGO and ET detectors, we also show a proposed “High Frequency” configuration for aLIGO [67].

and

$$\text{SNR}_{\text{ET}} \approx 2.5 \left( \frac{8 \times 10^{-25} \text{Hz}^{-1/2}}{\sqrt{S_n(f_{m=1})}} \right) \left( \frac{C_{21} r M}{10^{-4}} \right) \left( \frac{1.5 \text{kHz}}{f_{m=1}} \right)^2 \left( \frac{T_{m=1}}{100 \text{ms}} \right)^{1/2} \left( \frac{100 \text{Mpc}}{r} \right) \quad (4)$$

for the aLIGO zero-detuned high power configuration and the Einstein Telescope (ET) ET-D configuration [63], respectively. Here,  $S_n(f_{m=1})$  is the detector noise spectral density at the frequency of the one-arm mode and we adopt a mode lifetime of  $T_{m=1} = 100$  ms (order of magnitude consistent with some of our simulations) and distance to the source  $r = 10$  (100) Mpc for aLIGO (ET). Our SNR predictions are less optimistic than those in [41], but more optimistic than the predictions in [58]. However, we point out that these papers focused on quasicircular binaries and adopted different EOSs than we do. Note also that, as [41] pointed out, detection of a pre-merger NSNS signal will substantially lower the SNR requirements to claim a detection of a post-merger  $l = 2$ ,  $m = 1$  GW mode that is generated by a long-lived HMNS. Thus, the one-arm mode could potentially be detectable by aLIGO at 10 Mpc and by ET at 100 Mpc. However, if the one-arm mode survives intact for about 1 s, then aLIGO could possibly detect such a signal to  $\sim 30$  Mpc and the ET to  $\sim 300$  Mpc, which are similar distances other studies have found for the  $l = 2$ ,  $m = 2$  GW modes arising from post-merger oscillations (see e.g. [12]). Note also that for softer equations of state and unequal-mass mergers where  $C_{21} r M \sim 10^{-3}$  the SNR would be even larger, making the  $m = 1$  mode detectable for more distant events. Different aLIGO configurations such as the “High Frequency” one (see Fig. 10) could also help through lowering  $S_n(f_{m=1})$  by a factor of a few. Such configurations would be helpful in the future after observations have sufficiently constrained the nuclear equation of state. However, all these estimates depend on the assumptions that the source is observed edge-on (although note that the

(2,1) mode amplitude is maximized for an inclination  $\theta = \pi/3$ , at which the observed mode amplitude is about 30% larger than the edge-on ( $\theta = \pi/2$ ) case), and the signal frequency and amplitude are constant during the lifetime of the mode. Therefore, the estimates are rather optimistic because the mode frequency and amplitude are likely to change with time, especially since magnetic fields and neutrino emission could affect its properties. Nevertheless, our resolution study here and in [53, 19] demonstrate that at least when pure hydrodynamical effects are considered, with higher resolution the  $m = 1$  mode amplitude, once saturated, shows little to no signs of decay during the span of the simulations. Longer, high-resolution simulations that include detailed microphysics and magnetic fields are necessary to accurately determine the long-term evolution of the one-arm mode and detectability of the associated GWs.

These considerations indicate, as previous studies have also shown, that it is worth searching for near quasistationary signals following the merger of two neutron stars. Measurement of the frequency of these signals offers the potential to gain insights into the properties of the structure of the HMNS, and matter above the nuclear saturation density. Moreover, even the absence of a detection from a relatively nearby source will allow one to constrain the nuclear EOS, because the amplitude of the  $m = 1$  and  $m = 2$  modes vary significantly with EOS when other system parameters are fixed. Of course, degeneracies with other parameters would need to be considered, though a more thorough sampling of parameter space is required in order for a thorough investigation to be undertaken.

### 3.5. Properties of unbound matter and electromagnetic counterparts

In Fig. 11 we show the distribution of the asymptotic velocity of the ejected matter for several cases with periaapse  $r_p = 8M$ , two different mass ratios and various EOSs. From this plot one can see that, while there is substantial scatter, the stiffest equation of state (2H) results in more mass ejected at lower velocities than all other cases. In particular, amongst the  $r_p = 8.0M$  runs, the 2H case with  $q = 0.9$  gives the highest yield of  $\sim 0.015M_\odot$ . However, the largest amount in ejected matter comes from the  $q = 1.0$ ,  $r_p = 9.5M$ , 2H case with  $\sim 0.026M_\odot$  of ejected matter.

Based on these results we may estimate the properties of potential kilonovae powered by fission of short-lived radioactive nuclei produced through the r-process [42, 40]. Recent calculations of such processes suggest a rise time for kilonovae lightcurves of [4]

$$t_{\text{peak}} \approx 0.3 \left( \frac{M_{0,u}}{10^{-2}M_\odot} \right)^{1/2} \left( \frac{v}{0.2c} \right)^{-1/2} \text{ d}, \quad (5)$$

measured from the merger, and peak luminosities of

$$L \approx 1.6 \times 10^{41} \left( \frac{M_{0,u}}{10^{-2}M_\odot} \right)^{1/2} \left( \frac{v}{0.2c} \right)^{1/2} \text{ erg s}^{-1}. \quad (6)$$

We list more details about the properties of the ejecta as well as of potential electromagnetic counterparts in Table 3. Note that a  $L \sim 10^{41} \text{ erg s}^{-1}$  kilonova at the

**Table 3.** Properties of the unbound material from various cases considered in this work. Listed are the periaapse value of the initial orbit  $r_p$ , the equation of state, the dimensionless NS spins  $a_{\text{NS},1}$  and  $a_{\text{NS},2}$ , the unbound rest mass  $M_0$  in units of  $M_\odot/100$ , the rest-mass averaged asymptotic velocity  $\langle v_\infty \rangle$ , the total kinetic energy in units of  $10^{50}$  erg, the anticipated kilonovae rise time and luminosity in units of d and  $10^{41}$  erg/s, respectively, which we compute via Eqs. (5) and (6). We also include a lower resolution (2H,LR) run.

$r_p/M$	$q$	EOS	$a_{\text{NS},1}$	$a_{\text{NS},2}$	$M_{0,u}$	$\langle v_\infty \rangle$	$E_{\text{kin},50}$	$t_{\text{peak}}$	$L_{41}$
8.0	1.0	B	0.050	0.075	1.12	0.20	5.36	0.3	1.7
8.0	1.0	H	0.050	0.075	0.44	0.19	1.95	0.2	1.0
8.0	1.0	HB	0.050	0.075	0.84	0.19	3.65	0.3	1.4
8.0	1.0	2H	0.050	0.075	1.08	0.14	2.69	0.4	1.4
8.0	1.0	k1	0.050	0.075	0.24	0.20	1.18	0.1	0.8
8.0	1.0	k2	0.050	0.075	0.09	0.20	0.49	0.1	0.5
8.0	0.9	HB	0.050	0.050	0.56	0.21	3.01	0.2	1.2
8.0	0.9	2H	0.050	0.050	1.52	0.13	3.51	0.5	1.6
8.0	0.9	2H,LR	0.050	0.050	1.61	0.14	3.88	0.5	1.7
9.5	1.0	2H	0.050	0.075	2.56	0.17	8.45	0.5	2.4

edge of aLIGO’s *quasi-circular* NSNS horizon radius (at  $\sim 200$  Mpc) would translate to an r-band magnitude of 23.5 mag [4], one magnitude above the proposed LSST survey sensitivity [43]. Hence factors of a few difference in observed magnitude from such an intrinsic luminosity may be discernible, and together with the GW signal could allow one to constrain properties of the ejected matter, and consequently parameters of the NSNS system that merged. The highly eccentric NSNS encounters studied here may only be detectable out to roughly 1/10th the quasi-circular horizon distance [22] (larger impact parameter cases that result in multiple bursts could be heard further away if templates or power stacking methods are used, see [21, 70]). Of course, this means a significantly lower expected event rate, but also that the corresponding kilonova will have an apparent luminosity upwards of 100 times brighter than a 200 Mpc event.

#### 4. Conclusions and Future Work

In this work we considered eccentric mergers of binary neutron stars, concentrating on how the equation of state and mass-ratio affect the evolution of the resulting HMNS, and in particular the onset of the one-arm instability. Similarly to [58, 41], we find that the one-arm instability can occur in stars with stiff and soft EOSs, and that the location of the narrowly peaked signal in frequency encodes information about the NS EOS. We also find that binaries with disparate mass-ratios can more readily seed larger one-arm modes in the resulting HMNS star, in agreement with [41]. Furthermore, we discovered that in addition to toroidal and ellipsoidal HMNSs, double-core HMNSs can develop the  $m = 1$  instability. In this latter HMNS structure, strong  $m = 1$  density

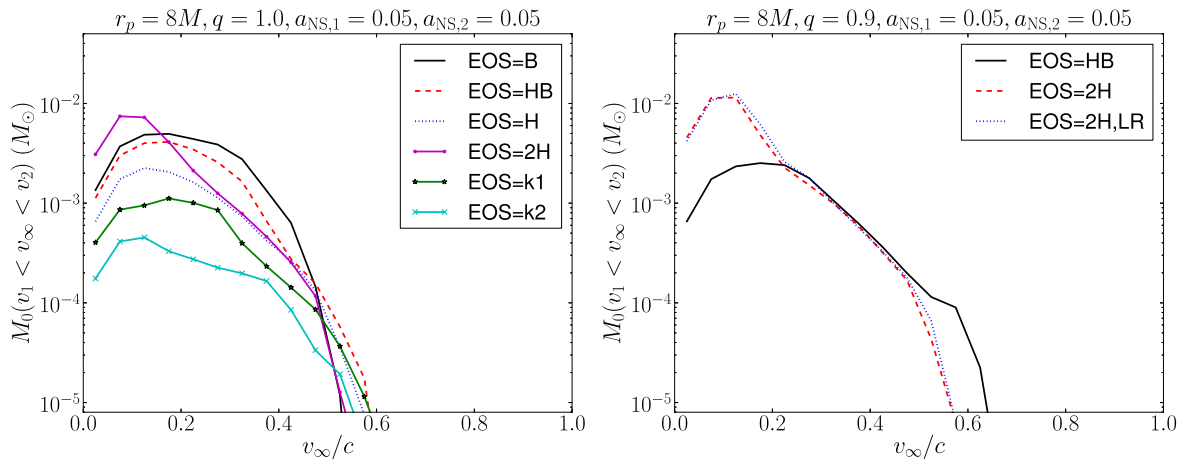


**Figure 11.** Distribution of the asymptotic velocity of unbound rest-mass, binned in increments of  $0.05c$ , and computed  $\sim 9.3$  ms post-merger for several  $r_p = 8M$  cases. Left:  $q = 1.0$  for various EOSs. Right:  $q = 0.9$  for 2 EOSs, where we also include the results from a lower resolution (LR) run for the 2H EOS case.

perturbations can already be present in the double-core phase, due to asymmetries in the two cores. Thus, correspondingly large  $l = 2, m = 1$  gravitational-wave modes can arise even before the dominance of a one-arm mode. In addition, our results suggest that stiffer equations of state produce HMNSs whose  $m = 1$  gravitational wave frequencies are lower than HMNSs formed with softer equations of state. This suggests that one should be able to find correlations between the frequency of the  $l = 2, m = 1$  GW mode and the EOS, in the same spirit as the correlations that have been discovered for the  $l = 2, m = 2$  mode [69, 71, 72, 6, 8, 7]. Thus, if gravitational waves from the one-arm instability are detected, they could in principle constrain the neutron star EOS. To make this robust, quantitative predictions will require the study of a larger suite of simulations with different equations of state, total masses and mass ratios, all of which will be pursued in future work.

Through some simple estimates of the signal-to-noise ratio for aLIGO and the future ET we concluded that, depending on the equation of state, the one-arm mode could potentially be detectable by aLIGO at  $\sim 10$  Mpc and by ET  $\sim 100$  Mpc. However, these estimates must be checked against long, high-resolution simulations that account for correct microphysics and magnetic fields, the impacts of which will be the subjects of forthcoming works.

Finally, we have computed the properties of dynamically ejected matter and find that at fixed periapse distance unequal-mass mergers eject more matter and the associated kilonovae signatures are brighter than in the case of equal-mass mergers (this is similar to the trends with mass ratio seen in quasi-circular merger simulations). The upcoming LSST survey with its exquisite sensitivity should be able to discern factors of a few difference in luminosity of kilonovae and hence constrain the properties of the ejected matter, and so potentially constrain the parameters of the NSNS system that

merged.

## Acknowledgments

We thank Stuart Shapiro for access to the equilibrium rotating NS code. This work was supported by NSF grant PHY-1607449, the Simons Foundation, NASA grant NNX16AR67G (Fermi), and by Perimeter Institute for Theoretical Physics. Research at Perimeter Institute is supported by the Government of Canada through the Department of Innovation, Science and Economic Development Canada and by the Province of Ontario through the Ministry of Research, Innovation and Science. Computational resources were provided by XSEDE/TACC under grant TG-PHY100053, TG-MCA99S008 and the Orbital cluster at Princeton University.

## References

- [1] B. P. Abbott et al. Gw151226: Observation of gravitational waves from a 22-solar-mass binary black hole coalescence. *Phys. Rev. Lett.*, 116:241103, Jun 2016.
- [2] B. P. Abbott et al. Observation of gravitational waves from a binary black hole merger. *Phys. Rev. Lett.*, 116:061102, Feb 2016.
- [3] L. Baiotti and L. Rezzolla. Binary neutron-star mergers: a review of Einstein’s richest laboratory. *ArXiv e-prints:1607.03540*, July 2016.
- [4] J. Barnes and D. Kasen. Effect of a High Opacity on the Light Curves of Radioactively Powered Transients from Compact Object Mergers. *Astrophys. J.*, 775:18, September 2013.
- [5] T. W. Baumgarte and S. L. Shapiro. *Numerical Relativity: Solving Einstein’s Equations on the Computer*. June 2010.
- [6] A. Bauswein and N. Stergioulas. A unified picture of the post-merger dynamics and gravitational wave emission in neutron-star mergers. *ArXiv e-prints:1502.03176*, February 2015.
- [7] A. Bauswein, N. Stergioulas, and H.-T. Janka. Exploring properties of high-density matter through remnants of neutron-star mergers. *ArXiv e-prints:1508.05493*, August 2015.
- [8] A. Bauswein, N. Stergioulas, and H.-T. Janka. Inferring neutron-star properties from gravitational-wave signals of binary mergers. *ArXiv e-prints:1503.08769*, March 2015.
- [9] E. Berger. Short-Duration Gamma-Ray Bursts. *Ann. Rev. Astron. Astroph.*, 52:43–105, August 2014.
- [10] S. Bernuzzi, D. Radice, C. D. Ott, L. F. Roberts, P. Moesta, and F. Galeazzi. How Loud Are Neutron Star Mergers? *ArXiv e-prints:1512.06397*, December 2015.
- [11] Sebastiano Bernuzzi, Tim Dietrich, Wolfgang Tichy, and Bernd Bruegmann. Mergers of binary neutron stars with realistic spin. *Phys.Rev.*, D89(10):104021, 2014.
- [12] J. A. Clark, A. Bauswein, N. Stergioulas, and D. Shoemaker. Observing gravitational waves from the post-merger phase of binary neutron star coalescence. *Classical and Quantum Gravity*, 33(8):085003, April 2016.
- [13] G. B. Cook, S. L. Shapiro, and S. A. Teukolsky. Rapidly rotating neutron stars in general relativity: Realistic equations of state. *Astrophys. J.*, 424:823–845, April 1994.
- [14] G. B. Cook, S. L. Shapiro, and S. A. Teukolsky. Rapidly rotating polytropes in general relativity. *Astrophys. J.*, 422:227–242, February 1994.
- [15] T. Dietrich, S. Bernuzzi, M. Ujevic, and B. Bruegmann. Numerical relativity simulations of neutron star merger remnants using conservative mesh refinement. *ArXiv e-prints:1504.01266*, April 2015.
- [16] T. Dietrich, N. Moldenhauer, N. K. Johnson-McDaniel, S. Bernuzzi, C. M. Markakis, B. Bruegmann, and W. Tichy. Binary Neutron Stars with Generic Spin, Eccentricity,



- Mass ratio, and Compactness - Quasi-equilibrium Sequences and First Evolutions. *ArXiv e-prints:1507.07100*, July 2015.
- [17] T. Dietrich, M. Ujevic, W. Tichy, S. Bernuzzi, and B. Bruegmann. Gravitational waves and mass ejecta from binary neutron star mergers: Effect of the mass-ratio. *ArXiv e-prints:1607.06636*, July 2016.
  - [18] K. Dionysopoulou, D. Alic, and L. Rezzolla. General-relativistic resistive-magnetohydrodynamic simulations of binary neutron stars. *ArXiv e-prints:1502.02021*, February 2015.
  - [19] W. E. East, V. Paschalidis, F. Pretorius, and S. L. Shapiro. Relativistic simulations of eccentric binary neutron star mergers: One-arm spiral instability and effects of neutron star spin. *Phys. Rev. D*, 93(2):024011, January 2016.
  - [20] W. E. East and F. Pretorius. Dynamical Capture Binary Neutron Star Mergers. *Astrophys. J. Lett.*, 760:L4, November 2012.
  - [21] William E. East, Sean T. McWilliams, Janna Levin, and Frans Pretorius. Observing complete gravitational wave signals from dynamical capture binaries. *Phys. Rev.*, D87(4):043004, 2013.
  - [22] William E. East and Frans Pretorius. Dynamical Capture Binary Neutron Star Mergers. *Astrophys. J.*, 760:L4, 2012.
  - [23] William E. East, Frans Pretorius, and Branson C. Stephens. Eccentric black hole-neutron star mergers: Effects of black hole spin and equation of state. *Phys. Rev. D*, 85:124009, Jun 2012.
  - [24] William E. East, Frans Pretorius, and Branson C. Stephens. Hydrodynamics in full general relativity with conservative adaptive mesh refinement. *Phys. Rev. D*, 85:124010, Jun 2012.
  - [25] William E. East, Fethi M. Ramazanoglu, and Frans Pretorius. Conformal Thin-Sandwich Solver for Generic Initial Data. *Phys. Rev.*, D86:104053, 2012.
  - [26] D. Eichler, M. Livio, T. Piran, and D. N. Schramm. Nucleosynthesis, neutrino bursts and gamma-rays from coalescing neutron stars. *Nature*, 340:126–128, July 1989.
  - [27] A. Endrizzi, R. Cioffi, B. Giacomazzo, W. Kastaun, and T. Kawamura. General Relativistic Magnetohydrodynamic Simulations of Binary Neutron Star Mergers with the APR4 Equation of State. *ArXiv e-prints:1604.03445*, April 2016.
  - [28] Z. B. Etienne, Y. T. Liu, S. L. Shapiro, and T. W. Baumgarte. General relativistic simulations of black-hole-neutron-star mergers: Effects of black-hole spin. *Phys. Rev. D*, 79(4):044024, February 2009.
  - [29] J. A. Faber and F. A. Rasio. Binary Neutron Star Mergers:1204.3858. *ArXiv e-prints:1204.3858*, April 2012.
  - [30] F. Foucart, R. Haas, M. D. Duez, E. O'Connor, C. D. Ott, L. Roberts, L. E. Kidder, J. Lippuner, H. P. Pfeiffer, and M. A. Scheel. Low mass binary neutron star mergers: Gravitational waves and neutrino emission. *Phys. Rev. D*, 93(4):044019, February 2016.
  - [31] R. Gold, S. Bernuzzi, M. Thierfelder, B. Brügmann, and F. Pretorius. Eccentric binary neutron star mergers. *Phys. Rev. D*, 86(12):121501, December 2012.
  - [32] R. Haas, C. D. Ott, B. Szilagyi, J. D. Kaplan, J. Lippuner, M. A. Scheel, K. Barkett, C. D. Muhlberger, T. Dietrich, M. D. Duez, F. Foucart, H. P. Pfeiffer, L. E. Kidder, and S. A. Teukolsky. Simulations of inspiraling and merging double neutron stars using the Spectral Einstein Code. *ArXiv e-prints:1604.00782*, April 2016.
  - [33] Brad M.S. Hansen and Maxim Lyutikov. Radio and x-ray signatures of merging neutron stars. *Mon. Not. Roy. Astron. Soc.*, 322:695, 2001.
  - [34] K. Hotokezaka, K. Kyutoku, H. Okawa, M. Shibata, and K. Kiuchi. Binary neutron star mergers: Dependence on the nuclear equation of state. *Phys. Rev. D*, 83(12):124008, June 2011.
  - [35] K. Hotokezaka, K. Kyutoku, Y.-i. Sekiguchi, and M. Shibata. Measurability of the tidal deformability by gravitational waves from coalescing binary neutron stars. *Phys. Rev. D*, 93(6):064082, March 2016.
  - [36] P. Jaranowski, A. Królak, and B. F. Schutz. Data analysis of gravitational-wave signals from spinning neutron stars: The signal and its detection. *Phys. Rev. D*, 58(6):063001, September 1998.

- [37] W. Kastaun and F. Galeazzi. Properties of hypermassive neutron stars formed in mergers of spinning binaries. *Phys. Rev. D*, 91(6):064027, March 2015.
- [38] K. Kiuchi, P. Cerdá-Durán, K. Kyutoku, Y. Sekiguchi, and M. Shibata. Efficient magnetic-field amplification due to the Kelvin-Helmholtz instability in binary neutron star mergers. *Phys. Rev. D*, 92(12):124034, December 2015.
- [39] K. Kiuchi, K. Kyutoku, Y. Sekiguchi, M. Shibata, and T. Wada. High resolution numerical relativity simulations for the merger of binary magnetized neutron stars. *Phys. Rev. D*, 90(4):041502, August 2014.
- [40] S. R. Kulkarni. Modeling Supernova-like Explosions Associated with Gamma-ray Bursts with Short Durations. *ArXiv e-prints:0510256*, October 2005.
- [41] L. Lehner, S. L. Liebling, C. Palenzuela, and P. Motl. The  $m = 1$  instability & gravitational wave signal in binary neutron star mergers. *ArXiv e-prints:1605.02369*, May 2016.
- [42] Li-Xin Li and Bohdan Paczynski. Transient events from neutron star mergers. *Astrophys. J.*, 507:L59, 1998.
- [43] LSST Dark Energy Science Collaboration. Large Synoptic Survey Telescope: Dark Energy Science Collaboration. *ArXiv e-prints:1211.0310*, November 2012.
- [44] S. T. McWilliams and J. Levin. Electromagnetic Extraction of Energy from Black-hole-Neutron-star Binaries. *Astrophys. J.*, 742:90, December 2011.
- [45] B. D. Metzger, A. Bauswein, S. Goriely, and D. Kasen. Neutron-powered precursors of kilonovae. *Mon. Not. R. Astron. Soc.*, 446:1115–1120, January 2015.
- [46] B. D. Metzger and E. Berger. What is the Most Promising Electromagnetic Counterpart of a Neutron Star Binary Merger? *Astrophys. J.*, 746:48, February 2012.
- [47] B. D. Metzger and C. Zivancev. Pair fireball precursors of neutron star mergers. *Mon. Not. R. Astron. Soc.*, 461:4435–4440, October 2016.
- [48] R. Mochkovitch, M. Hernanz, J. Isern, and X. Martin. Gamma-ray bursts as collimated jets from neutron star/black hole mergers. *Nature*, 361:236–238, January 1993.
- [49] R. Narayan, B. Paczynski, and T. Piran. Gamma-ray bursts as the death throes of massive binary stars. *Astrophys. J. Lett.*, 395:L83–L86, August 1992.
- [50] D. Neilsen, S. L. Liebling, M. Anderson, L. Lehner, E. O’Connor, and C. Palenzuela. Magnetized neutron stars with realistic equations of state and neutrino cooling. *Phys. Rev. D*, 89(10):104029, May 2014.
- [51] C. Palenzuela, L. Lehner, M. Ponce, S. L. Liebling, M. Anderson, D. Neilsen, and P. Motl. Electromagnetic and Gravitational Outputs from Binary-Neutron-Star Coalescence. *Physical Review Letters*, 111(6):061105, August 2013.
- [52] C. Palenzuela, S. L. Liebling, D. Neilsen, L. Lehner, O. L. Caballero, E. O’Connor, and M. Anderson. Effects of the microphysical Equation of State in the mergers of magnetized Neutron Stars With Neutrino Cooling. *ArXiv e-prints:1505.01607*, May 2015.
- [53] V. Paschalidis, W. E. East, F. Pretorius, and S. L. Shapiro. One-arm spiral instability in hypermassive neutron stars formed by dynamical-capture binary neutron star mergers. *Phys. Rev. D*, 92(12):121502, December 2015.
- [54] V. Paschalidis, Z. B. Etienne, and S. L. Shapiro. Importance of cooling in triggering the collapse of hypermassive neutron stars. *Phys. Rev. D*, 86(6):064032, September 2012.
- [55] V. Paschalidis, M. Ruiz, and S. L. Shapiro. Relativistic Simulations of Black Hole–Neutron Star Coalescence: The Jet Emerges. *Astrophys. J. Lett.*, 806:L14, June 2015.
- [56] Vasileios Paschalidis, Zachariah B. Etienne, and Stuart L. Shapiro. General relativistic simulations of binary black hole-neutron stars: Precursor electromagnetic signals. *Phys. Rev.*, D88:021504, 2013.
- [57] M. Ponce, C. Palenzuela, L. Lehner, and S. L. Liebling. Interaction of misaligned magnetospheres in the coalescence of binary neutron stars. *Phys. Rev. D*, 90(4):044007, August 2014.
- [58] D. Radice, S. Bernuzzi, and C. D. Ott. The One-Armed Spiral Instability in Neutron Star Mergers and its Detectability in Gravitational Waves. *ArXiv e-prints:1603.05726*, March 2016.

- [59] D. Radice, F. Galeazzi, J. Lippuner, L. F. Roberts, C. D. Ott, and L. Rezzolla. Dynamical Mass Ejection from Binary Neutron Star Mergers. *Mon. Not. R. Astron. Soc.*, May 2016.
- [60] J. S. Read, C. Markakis, M. Shibata, K. Uryū, J. D. E. Creighton, and J. L. Friedman. Measuring the neutron star equation of state with gravitational wave observations. *Phys. Rev. D*, 79(12):124033, 2009.
- [61] S. Rosswog, F. K. Thielemann, M. B. Davies, W. Benz, and T. Piran. Coalescing Neutron Stars: a Solution to the R-Process Problem? In W. Hillebrandt and E. Muller, editors, *Nuclear Astrophysics*, page 103, 1998.
- [62] M. Ruiz, R. N. Lang, V. Paschalidis, and S. L. Shapiro. Binary Neutron Star Mergers: A Jet Engine for Short Gamma-Ray Bursts. *Astrophys. J. Lett.*, 824:L6, June 2016.
- [63] B Sathyaprakash, M Abernathy, F Acernese, P Ajith, B Allen, P Amaro-Seoane, N Andersson, S Aoudia, K Arun, P Astone, B Krishnan, L Barack, F Barone, B Barr, M Barsuglia, M Bassan, R Bassiri, M Beker, N Beveridge, M Bizouard, C Bond, S Bose, L Bosi, S Braccini, C Bradaschia, M Britzger, F Brueckner, T Bulik, H J Bulten, O Burmeister, E Calloni, P Campsie, L Carbone, G Cella, E Chalkley, E Chassande-Mottin, S Chelkowski, A Chincarini, A Di Cintio, J Clark, E Coccia, C N Colacino, J Colas, A Colla, A Corsi, and A Cumming. Scientific objectives of einstein telescope. *Classical and Quantum Gravity*, 29(12):124013, 2012.
- [64] Y. Sekiguchi, K. Kiuchi, K. Kyutoku, and M. Shibata. Dynamical mass ejection from binary neutron star mergers: Radiation-hydrodynamics study in general relativity. *Phys. Rev. D*, 91(6):064059, March 2015.
- [65] Y. Sekiguchi, K. Kiuchi, K. Kyutoku, M. Shibata, and K. Taniguchi. Dynamical mass ejection from the merger of asymmetric binary neutron stars: Radiation-hydrodynamics study in general relativity. *ArXiv e-prints:1603.01918*, March 2016.
- [66] M. Shibata, T. W. Baumgarte, and S. L. Shapiro. The Bar-Mode Instability in Differentially Rotating Neutron Stars: Simulations in Full General Relativity. *Astrophys. J.*, 542:453–463, October 2000.
- [67] D. Shoemaker. Advanced LIGO Anticipated Sensitivity Curves, 2011. <https://dcc.ligo.org/cgi-bin/DocDB/ShowDocument?docid=2974>.
- [68] Nikolaos Stergioulas. Rotating stars in relativity. *Living Reviews in Relativity*, 3(6), 2003.
- [69] Nikolaos Stergioulas, Andreas Bauswein, Kimon Zagkouris, and Hans-Thomas Janka. Gravitational waves and nonaxisymmetric oscillation modes in mergers of compact object binaries. *ArXiv e-prints:1105.0368*, 2011.
- [70] Kai Sheng Tai, Sean T. McWilliams, and Frans Pretorius. Detecting gravitational waves from highly eccentric compact binaries. *Phys.Rev.*, D90(10):103001, 2014.
- [71] K. Takami, L. Rezzolla, and L. Baiotti. Constraining the Equation of State of Neutron Stars from Binary Mergers. *Physical Review Letters*, 113(9):091104, August 2014.
- [72] K. Takami, L. Rezzolla, and L. Baiotti. Spectral properties of the post-merger gravitational-wave signal from binary neutron stars. *Phys. Rev. D*, 91(6):064001, March 2015.